Review on performance optimization strategies and their mechanisms of bismuth layered-structured piezoelectric ceramics

Jieru Pu(蒲洁茹), Laihui Luo(罗来慧)

Citation: Chin. Phys. B. 35, 107701 (2026). DOI: 10.1088/1674-1056/ae82e2 | CSTR: 32038.14.CPB.ae82e2
http://cpb.iphy.ac.cn; http://iopscience.iop.org/cpb

What follows is a list of articles you may be interested in

Effect of heavy ion radiation on TDDB properties and lifetime prediction of high-*k* dielectric layers

Yan-Rong Cao(曹艳荣), Miao-Fen Li(李苗芬), Chen Ren(任晨), Zhi-Xian Zhang(张芝贤), Shuo Su(苏硕), Wei-Wei Zhang(张微微), You-Li Xu(徐由理), Ding-Qi Huang(黄碇起), Le Liu(刘乐), Ling Lv(吕玲), Pei-Pei Hu(胡培培), Liang-Wang(王亮), Xue-Feng Zheng(郑雪峰), Xiao-Hua Ma(马晓华), Yue-Hao(郝跃)
Chin. Phys. B. 35, 107702 (2026). DOI: 10.1088/1674-1056/ae39cf | CSTR: 32038.14.CPB.ae39cf

Characterization of large ferroelectric polarization and high-T_C in sol–gel deposited $PbTiO_3$-based perovskite thin films

Mengqi Ye(叶梦琪), Zhao Pan(潘昭), Weibin Song(宋伟宾), Jin Liu(刘锦), Xubin Ye(叶旭斌), Xin Xiong(熊心), Hui Liu(刘辉), Longlong Fan(樊龙龙), Nianpeng Lu(鲁年鹏), Ruilong Wang(王瑞龙), Youwen Long(龙有文)
Chin. Phys. B. 35, 027702 (2026). DOI: 10.1088/1674-1056/adf0e4 | CSTR: 32038.14.CPB.adf0e4

High-performance KNN-based piezoelectric ceramics for buzzer application

Cheng Xiong(熊城), Bosen Li(李博森), Zhongxin Liao(廖忠新), Yan Qiu(邱奕), Daqiang Gao(高大强)
Chin. Phys. B. 34, 047701 (2025). DOI: 10.1088/1674-1056/adb25e | CSTR: 32038.14.CPB.adb25e

Optimization of Skanavi model and its application to high permittivity materials

Hao Luo(罗昊), Xinrui Qin(秦新瑞), Kejia Geng(耿可佳), Cuncun Kong(孔存存), Pengfei Cheng(成鹏飞)
Chin. Phys. B. 34, 017702 (2025). DOI: 10.1088/1674-1056/ad9ba0 | CSTR: 32038.14.CPB.ad9ba0

Electrical analysis of inter-growth structured $Bi_4Ti_3O_{12}$–$Na_{0.5}Bi_{4.5}Ti_4O_{15}$ ceramics

Xiangping Jiang(江向平), Yalin Jiang(江亚林), Xingan Jiang(江兴安), Chao Chen(陈超), Na Tu(涂娜), Yunjing Chen(陈云婧)
Chin. Phys. B. 26, 077701 (2017). DOI: 10.1088/1674-1056/26/7/077701

TOPICAL REVIEW — A 40th Anniversary Celebration: Physics Research and Innovation at Ningbo University

Review on performance optimization strategies and their mechanisms of bismuth layered-structured piezoelectric ceramics

Jieru Pu(蒲洁茹) and Laihui Luo(罗来慧)[†]

School of Physical Science and Technology, Ningbo University, Ningbo 315211, *China*

(Received 23 April 2026; revised manuscript received 19 May 2026; accepted manuscript online 26 June 2026)

Bismuth layered-structured ferroelectrics (BLSFs) possess an exceptionally ultra-high intrinsic Curie temperature (generally above 600 °C) and excellent thermal stability, making them indispensable in high-temperature applications such as aerospace and nuclear power generation. However, the commonly prepared BLSF ceramics have low piezoelectric activity ($d_{33} < 10$ pC/N) and a high coercive field. This performance limitation originates from the spatial confinement of spontaneous polarization imposed by the two-dimensional layered structure as well as the oxygen vacancy defects introduced by bismuth volatilization during high-temperature sintering. This paper systematically reviews the recent research progress on the optimization method for the piezoelectric performance of BLSFs: 1) multi-element doping (A-site, B-site, A/B-site doping), which achieves a synergistic enhancement of piezoelectric response and intrinsic thermal stability by regulating the degree of lattice distortion, inhibiting oxygen vacancy migration, and inducing the formation of pseudo-tetragonal phase boundaries; 2) texturing processes including templated grain growth and hot pressing sintering achieve the statistical average limits of polycrystals by inducing oriented grain arrangement, resulting in anisotropic piezoelectric properties approaching those of single crystals; 3) high-entropy material design, which breaks the traditional constraint of polarization being confined to the *a*–*b* plane by introducing multi-principal elements to form two-dimensional amorphous defect layers, leading to additional out-of-plane polarization components and achieving a breakthrough in polarization flexibility and comprehensive performance. By analyzing the structural modification mechanisms of different systems, this paper reveals the synergistic enhancement effects of lattice distortion regulation, oxygen vacancy suppression, domain engineering, and high-entropy design on piezoelectric performance. This paper aims to provide strategic references for the rational design of high-performance high-temperature piezoelectric materials. Finally, it presents prospects for the piezoelectric performance and future applications of bismuth layer-structured piezoelectric ceramics.

Keywords: bismuth layered structure ferroelectrics, high-temperature piezoelectric ceramic, doping modification, texturing, high-entropy design

PACS: 77.84.–s, 77.80.B–, 77.90.+k, 85.50.–n

DOI: 10.1088/1674-1056/ae82e2 **CSTR:** 32038.14.CPB.ae82e2

1. Introduction

Piezoelectric ceramics are a type of functional ceramic material that possesses the piezoelectric effect. The piezoelectric effect refers to the phenomenon where the material generates electric charges when subjected to mechanical stress (positive piezoelectric effect), or undergoes deformation when an electric field is applied (reverse piezoelectric effect). This unique electro-mechanical coupling property enables piezoelectric ceramics to have extensive applications in fields such as sensors and transducers.[1,2] Among them, piezoelectric vibration sensors for high temperatures exceeding 350 °C have wide applications in aerospace, military weaponry, and petroleum exploration. Although traditional lead-based piezoelectric ceramics such as $Pb(Zr,Ti)O_3$ have a high piezoelectric coefficient, their Curie temperature is usually below 350 °C, which limits their application in high-temperature fields.[3–5] Therefore, there is an urgent need to develop high-performance piezoelectric materials with relatively high Curie temperature.

Aurivillius-type ceramics[6] or bismuth layer-structured ferroelectrics (BLSFs) exhibit several favorable properties, in particular, low dielectric permittivity and high Curie temperature, which make them potential materials for high-temperature device applications.[7] Bismuth layered materials are lead-free, thermally stable compounds with good ferroelectric and dielectric properties. Structurally, BLSFs consist of perovskite-like slabs of ABO_3 structure and fluorite-like $(Bi_2O_2)^{2+}$ layers regularly and alternately interleaved along the *c*-axis of the bismuth layer-structured oxide.[8] Their general formula is $(Bi_2O_2)^{2+}(A_{m-1}B_mO_{3m+1})^{2-}$. In this formula, the A-site is suitable for 12-coordinated monovalent, bivalent, and trivalent ions, such as Ca^{2+}, Sr^{2+}, Ba^{2+}, Bi^{3+}, La^{3+}, or their composite ions, while the B-site is suitable for octahedral coordination ions such as Ti^{4+}, Nb^{5+}, or their mixtures.[9,10] The integer m, generally referred to as the layer number, corresponds to the number of octahedral layers within the perovskite-like slabs $(A_{m-1}B_mO_{3m+1})^{2-}$ situated between the $(Bi_2O_2)^{2+}$ layers. Common systems with $m = 1$ in-

[†]Corresponding author. E-mail: luolaihui@nbu.edu.cn

© 2026 Chinese Physical Society and IOP Publishing Ltd. All rights, including for text and data mining, AI training, and similar technologies, are reserved.

clude Bi_2WO_6 (BW); those with $m = 2$ include Bi_3TiNbO_9 (BTN), $CaBi_2Nb_2O_9$ (CBN), $CaBi_2Ta_2O_9$ (CBTa), etc.; those with $m = 3$ include $Bi_4Ti_3O_{12}$ (BIT), etc.; and those with $m = 4$ include $SrBi_4Ti_4O_{15}$ (SBT), $Na_{0.5}Bi_{4.5}Ti_4O_{15}$ (NBT), $CaBi_4Ti_4O_{15}$ (CBT), etc.[11] The m value is closely related to the ferroelectric and piezoelectric properties of the material.[12,13] Generally speaking, the smaller the m value, the higher the Curie temperature, but the lower the piezoelectric activity. This unique layered structure endows the materials with a high Curie temperature, low dielectric loss, high resistivity, and excellent fatigue resistance, making them core candidate materials for piezoelectric sensors in extreme high-temperature environments such as aerospace, nuclear energy, national defense, transportation and geothermal exploration. The structures and brief application scenarios of BW, CBN, BIT, and CBT are shown in Fig. 1.

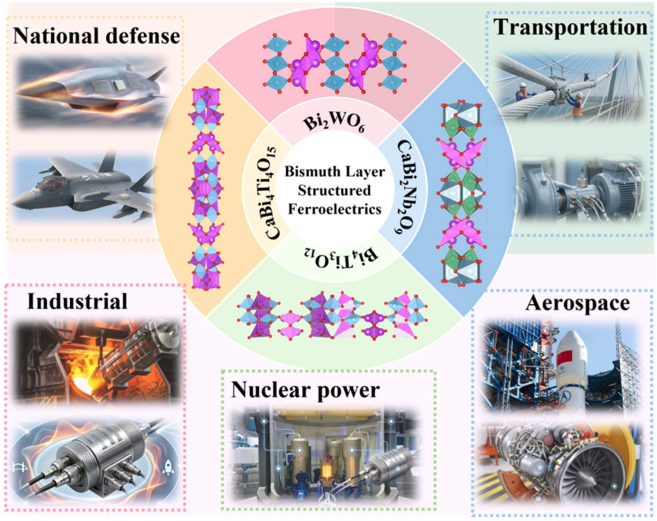

Fig. 1. Structures and brief application scenarios of BLSFs.

However, this type of material also has three significant drawbacks. First, its special crystal structure leads to a large c/a ratio, exhibiting significant anisotropy, with spontaneous polarization mainly confined to the a–b plane. This results in a significantly low piezoelectric coefficient d_{33} for ceramics with randomly oriented grains. Second, the Bi element tends to volatilize during high-temperature preparation, leading to the generation of a substantial number of oxygen vacancies within the crystal structure. This increases the carrier concentration, resulting in a significant reduction in electrical resistivity. Finally, due to their unique crystal structure, BLSFs readily form plate-like grains. This specific morphology introduces numerous pores between grains during the stacking process, which can create current pathways after sintering, consequently impeding the polarization process. These shortcomings severely restrict the widespread application of such ceramics in high-temperature piezoelectric devices. To enable the large-scale practical deployment of BLSFs, their piezoelectric performance and high-temperature electrical resistivity must be significantly enhanced. To achieve this goal, researchers have conducted extensive investigations into improving their piezoelectric properties.

2. Performance optimization strategies for BLSFs

BLSF ceramics possess a unique alternating layered structure that results in a high coercive field (> 120 kV/cm) and restricted polarization rotation. Consequently, their piezoelectric coefficients remain low (only about 6.0 pC/N). To address this challenge, researchers have proposed corresponding improvements for BLSFs through ion doping modification, texturing processes, and high-entropy design. The following section will discuss in detail the performance optimization strategies for BLSFs.

2.1. Doping strategy

Ion doping is the most fundamental and widely used optimization method, primarily achieved by adjusting crystal structure and defect chemistry. The essence of this approach lies in substituting the original ions with similar ionic radii and chemical valence states, thereby inducing lattice distortion and oxygen vacancy reduction to achieve enhanced electrical properties. The doping strategies can be further categorized into A-site doping, B-site doping, and A/B-site co-doping.

The A-site doping mainly uses lanthanide rare earth elements (La^{3+}, Nd^{3+}, Ce^{3+}, Yb^{3+}, Sm^{3+}, Eu^{3+}) and alkali metal ions (Na^{+}, K^{+}, Li^{+}) to replace the A-site ions such as Bi^{3+}, Ca^{2+}. When the valence states differ, various types of vacancies may emerge, resulting in a certain degree of lattice distortion. This effectively enhances the macroscopic electrical properties of BLSF ceramics. Research has revealed that the synergistic substitution of A-site Ca^{2+} ions in CBN ceramics with Na^{+} and Sm^{3+} ions can regulate its structure, electrical performance, and thermal stability properties. $Ca_{0.95}(Na, Sm)_{0.025}Bi_2Nb_2O_9$ (CBNS-0.025) ceramics exhibit a large piezoelectric coefficient ($d_{33} = 12.8$ pC/N), an ultrahigh Curie temperature ($T_C = 949$ °C), and an excellent direct current resistivity ($\rho = 4 \times 10^7$ Ω·cm at 500 °C).[14] By co-doping Li/Bi to enhance initial polarization and improve dielectric breakdown strength, the piezoelectric performance of CBT ceramics is synergistically enhanced.[15] As illustrated in Fig. 2(a), increasing the displacement of A-site ions enhances the intrinsic spontaneous polarization of the material at the atomic scale. Meanwhile, the PFM (piezoresponse force microscopy) results show a denser structure and weakened anisotropy of the material, reducing the pinning effect of grain boundaries on domain wall movement, making it easier for domains within the grains to be oriented under an external electric field. Li/Bi co-doped CBT ceramics also have higher

high-temperature resistivity (Fig. 2(a)). Furthermore, the introduction of Na/Pr/Ce ions at the A-site of CBT ceramics can effectively enhance the degree of lattice distortion, thereby facilitating spontaneous polarization and enhancing the intrinsic piezoelectric contribution. At the same time, the high density of domain walls facilitated the switching of electric domains, thereby enhancing the non-intrinsic piezoelectric contribution. Together, these effects led to an increase in the d_{33} value of this system to 22.3 pC/N, while the reduced oxygen vacancy concentration increased the temperature stability of the material.[16] The lattice distortion induced by doping enhanced the spontaneous polarization of the ceramics. The synergistic effects of both intrinsic and extrinsic factors contributed to the improved piezoelectric performance of the ceramics.

The B-site doping usually adopts the method of donor or acceptor substitution to control the oxygen vacancy concentration in the bismuth layered piezoelectric ceramics, thereby affecting the electrical properties of the material. Generally speaking, donor doping is considered to increase resistivity by injecting excess electrons to compensate for intrinsic hole carriers, whereas acceptor doping forms lattice defects and oxygen vacancies. Co-substituting Nb in CBN ceramics with Mo and Cr has achieved an optimal performance ($d_{33} = 15$ pC/N, $T_C = 939$ °C).[17] Mo/Cr co-doping significantly reduces oxygen vacancies and enhances the tetragonal nature of the lattice structure, thereby improving the piezoelectricity, thermal stability and resistivity of ceramics. Composite ions ($Cr_{1/3}/Ta_{2/3}$) formed by low-valence Cr^{3+} and high-valence Ta^{5+} are introduced into the B-site of BIT. This approach effectively suppresses oxygen vacancies, thereby synergistically enhancing the overall electrical performance of the material. As shown in Fig. 2(b), the original layered structure remains preserved after Cr/Ta doping, which is a typical characteristic of Aurivillius class of compounds.[18] The prepared $Bi_4Ti_{2.97}(Cr_{1/3}Ta_{2/3})_{0.03}O_{12}$ (BTCT3) ceramic exhibits a high piezoelectric coefficient ($d_{33} = 26$ pC/N) and a high Curie temperature ($T_C = 687$ °C). Furthermore, this composition achieves significantly increased resistivity ($\rho = 2.8 \times 10^6$ Ω·cm at 500 °C) and excellent piezoelectric stability up to 600 °C. By substituting Ti at the B-site of NBT ceramics with Nb and Co, respectively, NBT ceramics with a T_C of 666 °C and d_{33} of 30 pC/N, as well as T_C of 690.2 °C and d_{33} of 22 pC/N, were obtained.[19,20] B-site doping increases the b/a lattice parameter ratio, leading to distortion of the TiO_6 octahedra and a structural transition from orthorhombic to tetragonal phase, thereby improving the ferroelectric properties.

The A-site ions have relatively large radii, which provides convenience for the design of the crystal structure and is an effective way to enhance the electrical properties of BLSF ceramics. However, improving piezoelectric performance through A-site ion substitution often comes at the cost of sacrificing Curie temperature. In contrast, although B-site ion substitution can weaken the pinning effect of oxygen vacancies, due to the smaller radius of B-site ions, its modification effect is not very pronounced. The co-substitution at both A and B sites combines the advantages of both, capable of simultaneously achieving high Curie temperatures and high piezoelectric performance.[21] For ultrahigh-temperature piezoelectric applications, A-site Li/Nd co-doping and B-site Sc/W co-doping were employed in CBN ceramics. By elucidating the effects of cation disordering, defect dipole reorientation, and domain structure on the electrical properties, CBN-based ceramics with superior performance ($d_{33} = 20.6$ pC/N, $T_C = 908$ °C) to conventional materials were successfully fabricated.[22] An A/B-site co-doping strategy involving the simultaneous introduction of Li/Pr at the A site and Bi/Sc at the B site was adopted to synergistically optimize the comprehensive performance of CBN ceramics, rendering them highly promising piezoelectric materials for high-temperature sensing applications.[23] As shown in Fig. 2(c), doping exerts a significant influence on the crystal structure and defect chemistry of the CBN ceramics. Notably, no obvious degradation in piezoelectric performance was observed for all compositions upon annealing at temperatures up to 800 °C. Moreover, distinct 180° domains and small belt-shaped 180° DWs along with head-to-head or tail-to-tail were clearly observed, which contribute to the enhanced piezoelectric properties ($d_{33} = 18.2$ pC/N, $T_C = 938$ °C).[23] Excellent piezoelectric performances ($T_C = 675$ °C, $d_{33} = 32$ pC/N) were obtained in NBT ceramics via replacing the Na ions at the A site with Li/Ce/Bi ions and the Ti ions at the B site with Sc ions.[24] Remarkably, after annealing the sample in an oxygen atmosphere, the d_{33} value increased to 37 pC/N, which is attributed to the reduction of oxygen vacancy concentration. Meanwhile, all samples exhibited good piezoelectric stability. Through the experimental approach of Er^{3+} doping at the A-site combined with Nb^{5+}/W^{5+} co-doping at the B-site, BIT-based ceramics with high piezoelectric performance ($d_{33} = 36$ pC/N), high Curie temperature (657 °C), high resistivity (4.2×10^6 Ω·cm at 500 °C), and high-precision temperature sensing capability over a wide temperature range were successfully fabricated.[25] In summary, A/B-site co-doping effectively enhances the piezoelectric activity and resistivity of ceramics while simultaneously tuning the Curie temperature and temperature stability, making chemical doping at the A/B sites of BLSFs an effective strategy for improving the piezoelectric coefficient and resistivity at high temperatures.

In a word, ion doping modification can increase the piezoelectric coefficient d_{33} of BLSF ceramics from 6 pC/N to 15–45 pC/N approximately, with a relatively small sacrifice to

the Curie temperature T_C. At the same time, it significantly enhances the high-temperature resistivity by reducing oxygen vacancies. This strategy is simple in process, low in cost, and easy to scale up for production, making it the most practical performance optimization method for current industrial applications.

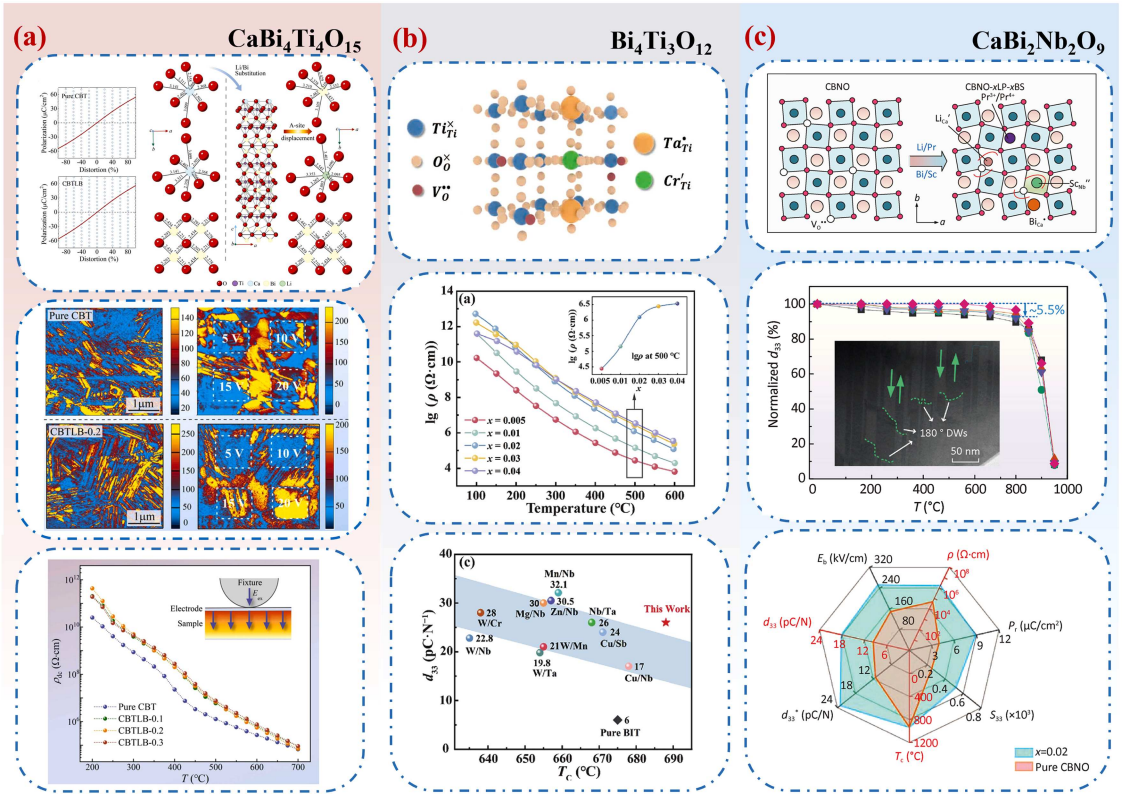

Fig. 2. The performance improvement of BLSFs after doping at A-site, B-site, and A/B-site. (a) The local atomic structure of the pure CBT phase and the doped CBT phase (theoretical calculation results); VPFM (vertical piezoresponse force microscopy) images of pure CBT ceramics and $Ca_{0.8}(Li_{0.5}Bi_{0.5})_{0.2}Bi_4Ti_4O_{15}$ ceramics; the temperature dependence of ρ_{dc}.[15] (b) Schematic diagram of the crystal structure after doping; temperature dependence of logarithmic resistivity of BTCT100x ceramics; the relationship between d_{33} and T_C in BIT-based ceramics.[18] (c) Schematic illustration of the microstructure of CBN-based ceramics after doping, along with comparisons of temperature stability and comprehensive performance.[23]

2.2. Texture technology

Texturing processes mainly refer to grain orientation techniques. By achieving high alignment of spontaneous polarization directions (within the a–b plane), this represents one of the most effective methods to overcome two-dimensional polarization limitations and substantially enhance piezoelectric properties. These techniques mainly include templated grain growth (TGG), hot pressing sintering (HPS), spark plasma sintering (SPS), and two-step sintering (TSS). Through controlling the preferred orientation of grains along the (00l) direction and fully exploiting piezoelectric anisotropy, texturing processes can increase d_{33} by 3 to 5 times.[26–28]

The TGG method is an advanced processing technique used to prepare ceramics with strong anisotropic textures. This technology involves introducing template grains with a specific orientation into a ceramic matrix. By leveraging the anisotropic growth characteristics of the grains, it induces the matrix grains to grow oriented along the crystallographic direction of the template grains during the sintering process, thereby obtaining a ceramic material with a highly textured microstructure. Crystals with a layered structure, synthesized via hydrothermal or molten salt methods, are typically used as template grains. The hydrothermal method utilizes a high-temperature and high-pressure hydrothermal environment to promote crystal growth, yielding template grains with high crystallinity and regular morphology. The molten salt method accelerates solid-state reactions and crystal growth by using low-melting-point salts as a reaction medium at high temperatures, making it suitable for large-scale synthesis.[26,29,30] The specific process is shown in Fig. 3(a). Currently, there are increasing reports on the texturing processes of BLSFs. For example, Nb-ion-doped BIT textured ceramics have been prepared, increasing the d_{33} value to 30 pC/N.[31] It has also been found that the use of fine precursor powder helps enhance the density of the ceramics and maintains excellent thermal stability at a high temperature of 600 °C. Luo *et al.* have prepared textured CBN-based ceramics by the TGG method combined with Na/Sm co-doping. The Na/Sm co-doping introduces atomic-scale disorder and local structural heterogeneity, and the significant reduction in the relative displacement of Ca atoms with respect to Nb atoms all contribute to the enhancement of piezoelectric performance (Fig. 3(b)). TEM reveals the presence of high-density striped nanodomains in the textured samples, with domain walls being curved but ir-

regular, a domain structure that facilitates domain switching under an external electric field (Fig. 3(c)). The as-prepared ceramics achieve a piezoelectric coefficient $d_{33} > 30$ pC/N and $T_C > 950$ °C (Fig. 3(d)).[32]

HPS requires pre-filling all powder particles into a hot-press die, enabling the simultaneous application of uniaxial or biaxial mechanical pressure during the ceramic sintering stage. This externally applied pressure serves as an additional driving force beyond conventional thermal sintering, effectively promoting interparticle contact and mass transport. Consequently, it reduces the sintering temperature while ensuring high densification, and also offers the possibility of controlling the preferred grain orientation.[33] The main process steps include reaction-molding-degumming and sintering (Fig. 4(a)). HPS induced preferred orientation in the CBTa-based ceramics,[28] effectively aligning the polar domains while maintaining the layered perovskite structure. This optimization significantly enhanced the piezoelectric response ($d_{33} = 21.8$ pC/N) and DC resistivity ($> 1.11 \times 10^7$ Ω·cm at 600 °C) without compromising the Curie temperature T_C (922 °C). Notably, the textured ceramics retained 95% of their initial piezoelectric performance after depolarization at 900 °C for 2 h, highlighting their exceptional thermal stability. A piezoelectric ceramic BCTNTW with high texture degree, high density, and excellent piezoelectric properties was successfully prepared by combining the chemical substitution method (Ce, W, Ta) with HPS.[34] As shown in Fig. 4(b), when the sample is cut in different directions, the sample cut in the vertical pressure direction (BCTNTW-Per) exhibits a (100) preferred orientation and a more easily reversible domain structure, thereby achieving excellent comprehensive performance; secondly, the HPS method forms larger-sized and more evenly distributed micrometer domains, and endows the sample with uniform local piezoelectric response (Fig. 4(c)), thereby explaining the mechanism of the improvement in the piezoelectric performance of textured ceramics at the microscopic scale. The obtained piezoelectric constant d_{33} reaches 27 pC/N (twice that of traditional sintered samples), the remanent polarization Pr reaches 17.7 μC/cm^2, the T_C is as high as 890 °C, the resistivity at 600 °C remains 1.6×10^5 Ω·cm, and it can still maintain more than 90% of the initial d_{33} value after 800 °C annealing (Fig. 4(d)).

SPS is another ceramic preparation process, which is similar to HPS, but the two methods differ in their heating approaches. While applying pressure to the sample, the latter uses pulsed electric current to heat and sinter the powder particles. It offers advantages such as uniform heating, fast heating rates, low sintering temperatures, and short sintering times.[35] It has been reported in the literature that the piezoelectric performance of BLSFs can be enhanced by the SPS method. For example, highly textured sodium bismuth titanate ceramics were prepared. This ceramic exhibits a high degree of preferential orientation and a good piezoelectric constant d_{33} (35.8 pC/N), which is more than twice that of conventionally sintered NBT (15.8 pC/N).[36]

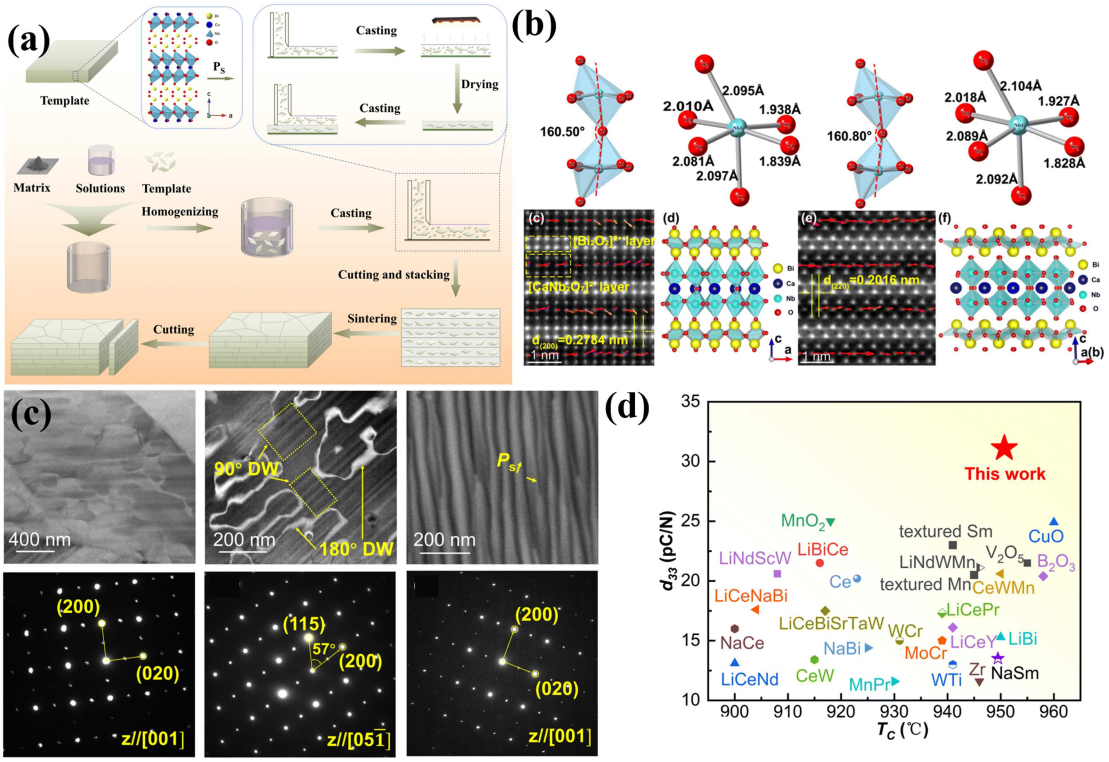

Fig. 3. (a) Schematic diagram of the TGG preparation process;[32] (b) structural evolution of NbO_6 octahedra in CBN and CBNNS ceramics and the relative displacement of Ca atoms compared to Nb atoms in the perovskite layer; (c) TEM images of textured CBNNS ceramics and corresponding selected-area electron microscope images; (d) comparison of d_{33} and T_C of textured CBNNS ceramics with other representative CBN-based ceramics.[32]

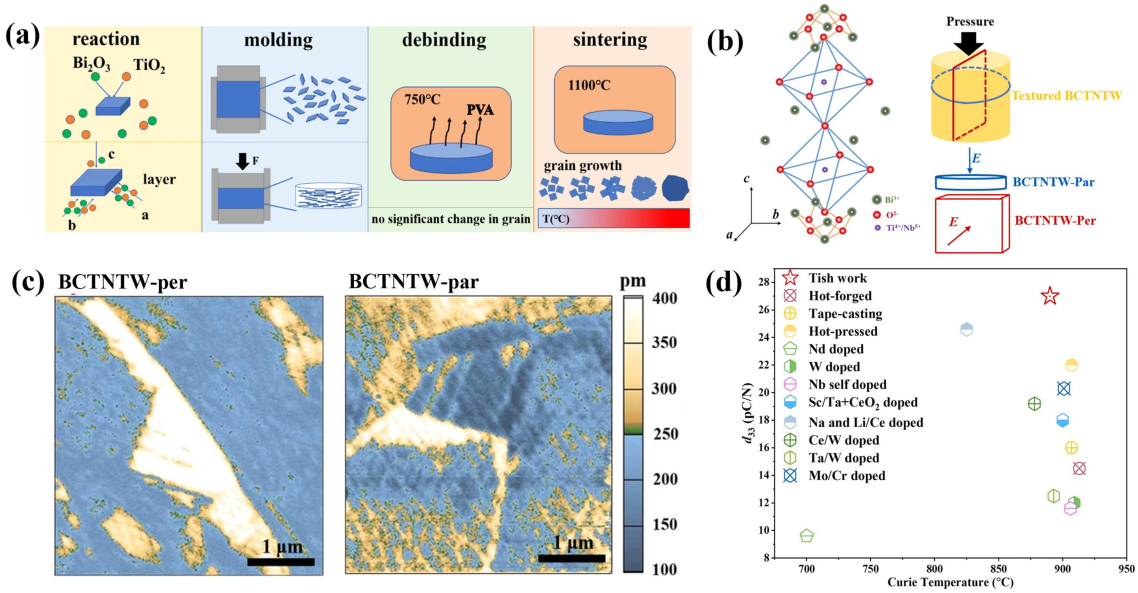

Fig. 4. (a) Schematic diagram of the HPS preparation process;[37] (b) schematic diagram of BTN crystal structure and illustrations of BCTNTW ceramics cut perpendicularly and parallel to the pressure direction; (c) the domain structure of BCTNTW ceramics; (d) T_C and d_{33} of BTN-based ceramics with different ion doping and processing techniques.[34]

The textured technology effectively overcomes the two-dimensional limitation of the spontaneous polarization of bismuth layered materials, which is confined to the *a*–*b* plane, by inducing the crystal grains to align along a specific direction, and improves d_{33} to a certain extent. However, this strategy requires additional template grain growth preparation or pressurized sintering equipment, resulting in a more complex process and higher cost than the traditional doping method. Compared with the doping strategy, texturing can achieve a higher upper limit of piezoelectric performance, but it is not conducive to low-cost large-scale production.

2.3. High-entropy design

At present, high entropy has emerged as an effective and flexible strategy to enhance the physical properties of ferroelectrics through the careful design of local polarization configurations. According to thermodynamic principles, the Gibbs free energy can be expressed as $\Delta G = \Delta H - T\Delta S$.[38] The high-entropy strategy significantly increases the configurational entropy of the system by introducing multiple principal elements, thereby lowering the free energy at high temperatures and stabilizing the solid solution phase. Additionally, it leverages the entropy increase effect to induce local structural distortions, thereby significantly enhancing the comprehensive electrical properties of the material.[39] Furthermore, the high-entropy strategy exhibits distinct advantages in designing excellent comprehensive physical properties via the cocktail effect, and can also be employed to design local polarization disorder behavior.[40–42] Qi[43] pioneered the introduction of the high-entropy strategy into the design of high-temperature piezoelectric ceramics. By incorporating heteroatoms such as Na^+, Ti^{4+}, and Ta^{5+} into the CBN ceramic matrix, they developed a high-entropy high-temperature piezoelectric ceramic material $Ca_{1/3}(Na_{0.5}Bi_{0.5})_{1/3}(Bi_{7/3}Ti_{1/3}Nb_{1/3}Ta_{4/3})O_9$. As shown in Fig. 5(a), the high-entropy sample exhibits an alternating arrangement of perovskite-type $(CaNb_2O_7)^{2-}$ layers and bismuth $(Bi_2O_2)^{2+}$ layers stacked along the (001) axis. The well-crystallized Aurivillius phase of CBN was confirmed using atomic-resolution high-angle annular dark-field scanning transmission electron microscopy (HAADF-STEM). The material achieved a piezoelectric coefficient ranging from 20.6 pC/N to 31.5 pC/N and a high DC resistivity of 10^6 Ω·cm at 750 °C, far superior to conventional CBN-based ceramics. The coercive field was significantly reduced, while the remanent polarization increased, facilitating poling treatment.

Another A/B-site substituted CBTa (with Li/Na/Ce at the A-site and Nb/W/Ti at the B-site) system based on a high-entropy strategy significantly enhances the piezoelectric constant d_{33} from 5.4 pC/N in pure CBTa ceramic to 12.1 pC/N for $Ca_{0.74}Li_{0.03}Na_{0.1}Ce_{0.04}Bi_{2.09}Ta_{1.4}Nb_{0.2}W_{0.2}Ti_{0.2}O_9$ (CLNCBTaNWT-2) ceramics (Fig. 5(b)),[44] which is attributed to the effective introduction of doping ions enhancing ferroelectricity. PFM measurements observed 180° and 90° domain walls, indicating that the domains in CLNCBTaNWT-2 ceramics exhibit more facile switching behavior. Concurrently, ultrasonic experiments showed that the signal-to-noise ratios for the symmetric zero-order mode (S_0) and antisymmetric zero-order mode (A_0) generated by the obtained CLNCBTaNWT-2 ceramics reached 12.2 dB and 19.7 dB, respectively, with performance stable up to 400 °C. These results demonstrate that CBTa-based ceramic systems designed using a high-entropy strategy hold promising application prospects in high-temperature ultrasonic structural health monitoring.

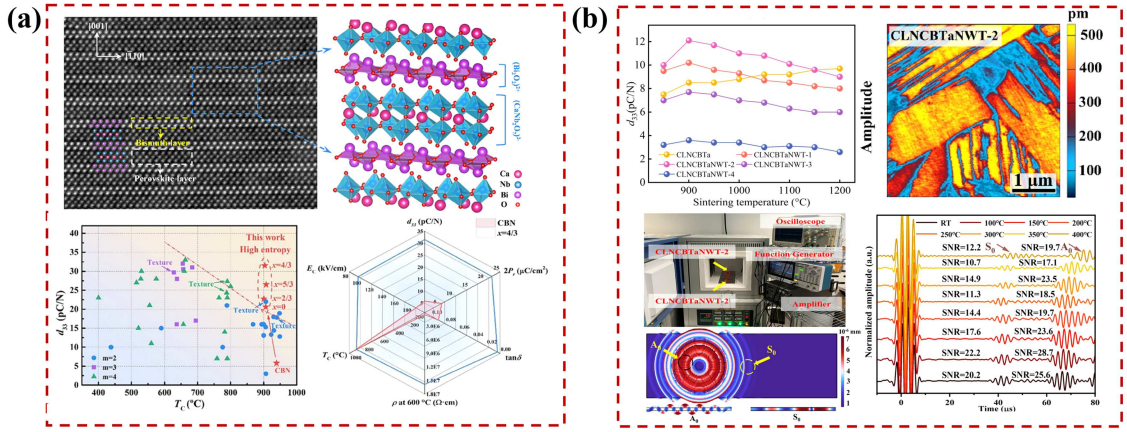

Fig. 5. (a) HAADF-STEM images of CBN; d_{33} and T_C values of several typical bismuth-based layered structure ceramics were compared, the comprehensive performance of CBN and high-entropy $x = 4/3$ samples.[43] (b) d_{33} values of CLNCBTa and CLNCBTaNWT-10x ($x = 0.1$–0.4) ceramics with different sintering temperatures; PFM images of the optimal performance of CLNCBTaNWT-2; experimental settings and verifications were conducted for ultrasonic detection in A_0 and S_0 modes, and voltage signals at different temperatures were received.[44]

Compared with the first two optimization strategies, the introduction of high-entropy design results in the best comprehensive performance of BLSF ceramics. However, the selection and optimization of high-entropy components rely on a large number of trial-and-error experiments, and the process window is narrow, making the preparation rather difficult. Additionally, the introduction of high entropy gives it a significant advantage in high-temperature resistivity, and the improvement in the piezoelectric coefficient is considerable.

3. Piezoelectric enhancement mechanism

Generally, doping ions enhance piezoelectric performance through two primary mechanisms. The first involves substituting B-site ions with larger-radius ions. The increased ionic radius induces distortion in the BO_6 octahedra, enhancing the orthorhombic distortion of the lattice (manifested as the b/a ratio), which directly strengthens the spontaneous polarization. The second mechanism utilizes metal ions doped at the A-site to induce ionic shifts, effectively reducing the lamellar orientation preference of the ceramics. This promotes a more random grain orientation, which, counterintuitively, facilitates the alignment of a greater number of grain polarization directions with the external electric field. As shown in Fig. 6(a), the rotation distortion of the TiO_6 octahedra in the NBT ceramic doped with $Nb_{1/2}Cr_{1/2}$ is significantly amplified. This pronounced rotational modification may play a key role in enhancing the piezoelectric performance of the NBT-NC6 sample.[45] Furthermore, the spontaneous polarization for BLSFs is strictly confined within the *a*–*b* plane of the crystal lattice. A fundamental change occurs when processing techniques are employed to achieve grain texturing, aligning the *a*–*b* planes of grains parallel to the direction of the applied electric field. In this scenario, the originally confined polarization direction within the grains becomes aligned with the external field, significantly improving poling efficiency. During the poling process, the external electric field can directly act on the intrinsic polarization direction of these grains, driving domain wall motion and polarization switching.

When the donor ions or specific atmospheres are applied for treatment, it can effectively reduce the concentration of oxygen vacancies, and the pinning effect of domain walls is significantly weakened. The domain walls regain their mobility and can freely move under an external electric field. More domains can participate in the polarization switching. This not only makes the polarization process more complete, but also reduces the coercive field, enabling the material to reach saturation polarization at a lower electric field. It is worth noting that the regulation of oxygen vacancies is not limited to simply reducing the concentration. In some doping strategies, the oxygen vacancies generated by the acceptor ions are bound near the defect centers, forming defect dipoles. These bound oxygen vacancies do not participate in long-range conduction and will not freely migrate to the domain walls to form pinning, thereby achieving the reduction of effective oxygen vacancy concentration. The formation of defect dipole pairs (Na'_{Ca}–V''_O) in Na^+-doped CBN ceramics effectively reduces the concentration of free oxygen vacancies through an electrostatic binding effect, while simultaneously stabilizing the ferroelectric phase. As a result, high piezoelectricity, high Curie temperature, and high electrical resistivity are achieved concurrently. The XPS experiment (Fig. 6(b)) provides corresponding evidence for this mechanism.[46]

On the other hand, high-density nanoscale strip-like domains and domain walls can be observed in the samples with better performance. The nanodomains have a higher density of domain walls, meaning there are more movable interfaces within a unit volume. The domain walls also contribute to the diversity of the polarization direction and the coordination of domain flipping. The optimization of these domain structures enables the material to exhibit higher remanent polarization Pr and a larger piezoelectric coefficient on a macroscopic scale.

As shown in Fig. 6(c), the introduction of Ta/Sb ions into the BIT ceramic modifies its domain structure, resulting in a stripe domain configuration with lower domain wall energy and enhanced mobility. This promotes polarization switching and stress-induced charge output, thereby significantly improving the piezoelectric response.[47]

High-entropy design primarily enhances piezoelectric performance by introducing two-dimensional amorphous defects and local chemical disorder, which excite additional out-of-plane polarization components while simultaneously reducing the polarization switching energy barrier. Through atomic-resolution HAADF-STEM combined with polarization vector mapping and elemental analysis, the formation of two-dimensional defects in high-entropy design CBN ceramics at the atomic scale is revealed (Fig. 6(d)).[43] Furthermore, the lattice distortion around these defects generates out-of-plane polarization components that are not allowed in the conventional Aurivillius structure, making the polarization more flexible. As a result, the ceramic responds more readily under an external electric field, macroscopically manifesting as a lower coercive field and a higher piezoelectric coefficient.

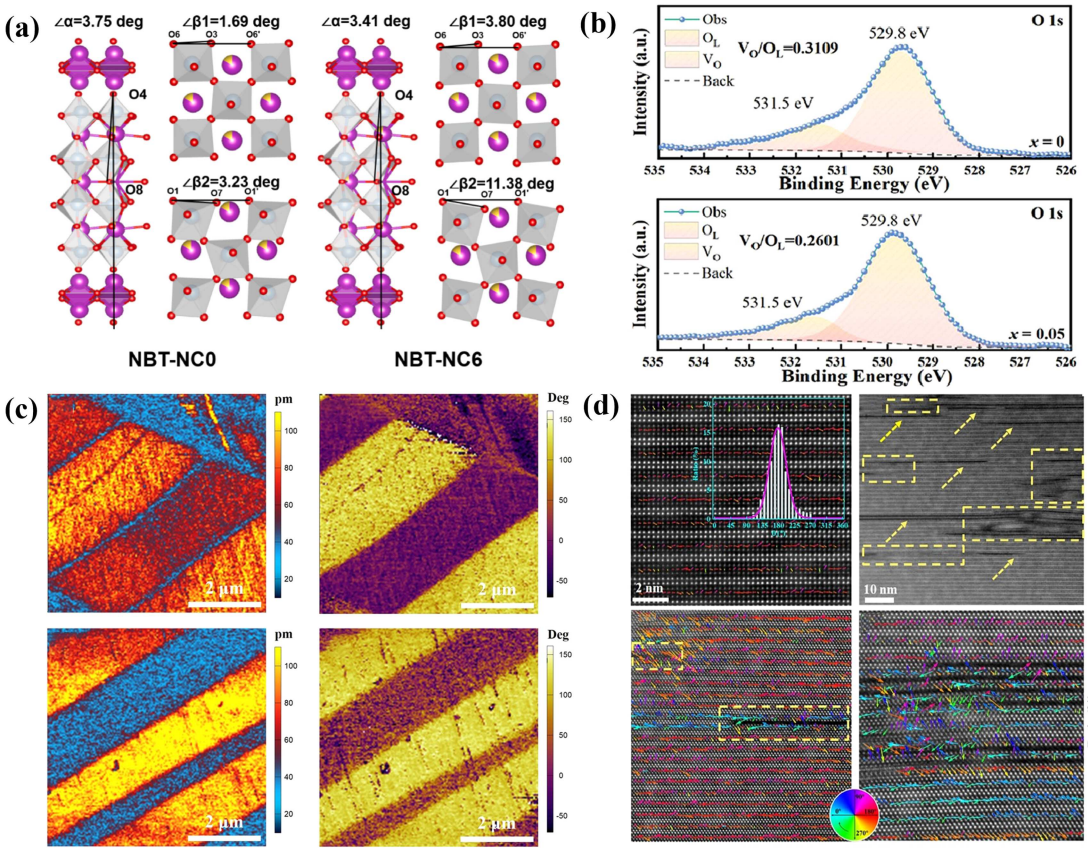

Fig. 6. Mechanisms for performance enhancement of BLSFs. (a) Tilt and rotation degrees of TiO_6 octahedra in NBT-NC0 and NBT-NC6 ceramics,[45] (b) XPS O 1s spectra of CNBN-0 and CNBN-0.05,[46] (c) VPFM amplitude and phase images of BCTMTS-0 and BCTMTS-3 ceramics,[47] (d) atomic-scale characterization of local structural evolution using high-entropy engineering about CBN.[43]

4. Conclusion and prospect

This review has synthesized key optimization strategies for enhancing the piezoelectric performance of BLSFs, addressing their intrinsic limitation of low piezoelectric activity despite ultra-high Curie temperatures. The performance optimization strategies for bismuth layer-structured piezoelectric ceramics have evolved from single doping modification to a new stage of multi-dimensional collaborative regulation. Domain engineering provides new mechanisms for further breaking through performance limits, and opens up new pathways for the high-performance application of low-piezoelectric-activity materials. Methods like templated grain growth and hot-press sintering induce grain orientation, aligning the spontaneous polarization direction with the applied electric field. This overcomes the two-dimensional polarization confinement and can enhance d_{33} effectively, with textured ceramics achieving values exceeding 30 pC/N. The high-entropy strategy is also beneficial for grain refinement processes, mechanical property improvement, and entropy stabilization effects, opening up opportunities for designing high-entropy ferroelectric materials with novel polarization configurations and excellent performance (entropy-stabilized oxides, high-entropy ceramics). Therefore, its piezoelectric performance is being continuously improved, and it is expected to achieve a critical leap from a candidate material to a core material in fields such as aerospace high-temperature sensors, high-

frequency communication devices, and lead-free environmentally friendly alternatives in the future.

Although ion doping, texturing, and high-entropy strategies have significantly improved the performance of bismuth layered piezoelectric ceramics, the traditional "trial-and-error" experimental methods are time-consuming and labor-intensive, and it is difficult to comprehensively explore the complex composition space corresponding to ceramics composed of multiple principal components. In addition, to understand the intrinsic relationship between local distortion, oxygen vacancy distribution, and macroscopic performance in BLSF ceramics, theoretical simulations that go beyond conventional computing capabilities are required. Machine learning potential functions can play a key role in this field. By generating datasets through high-throughput first-principles calculations and training machine learning potential functions, it is possible to quickly and accurately predict the formation energy, lattice distortion degree, oxygen vacancy formation energy, and intrinsic piezoelectric response of different element combinations at different ratios. By using machine learning potential functions, large-scale BLSF ceramics supercell models containing thousands or even tens of thousands of atoms can be constructed and large-scale molecular dynamics simulations can be conducted.

Future research should focus as much as possible on the deep integration of atomic-scale structural modulation, high-entropy design, intelligent preparation processes, and device engineering. At the same time, greater emphasis should be placed on evaluating the long-term reliability of devices under actual service conditions. There is an urgent need to develop *in-situ* operational measurements, that is, real-time tracking of piezoelectric responses during thermal cycling, mechanical vibration, or humidity exposure. Accelerated aging tests, which apply elevated temperatures or cyclic electric fields over a relatively short period, can be used to predict the service lifetime of BLSF ceramics. Establishing standardized testing protocols for such materials will be a crucial step toward promoting their practical applications in fields such as aerospace and nuclear energy.

References

[1] Turner R, Fuierer P A, Newnham R and Shrout T R 1994 *Appl. Acoust.* **41** 299
[2] Damjanovic D 1998 *Curr. Opin. Solid State Mater. Sci.* **3** 469
[3] Jaffe B, Roth R and Marzullo S J 1954 *J. Appl. Phys.* **25** 809
[4] Dong Y, Zou K, Liang R and Zhou Z J 2023 *Prog. Mater. Sci.* **132** 101026
[5] Xin R, Wang Y, Fang Z, Zheng F, Gao W, Fu D, Shi G, Liu J Y and Zhang Y 2024 *Chin. Phys. B* **33** 087701
[6] Aurivillius B 1949 *Arkiv Kemi.* **1** 463
[7] Zhang S and Yu F 2011 *J. Am. Ceram. Soc.* **94** 3153
[8] Newnham R E, Wolfe R W and Dorrian J F 1971 *Mater. Res. Bull.* **6** 1029
[9] Zhou Z, Li Y, Hui S and Dong X 2014 *Appl. Phys. Lett.* **104**
[10] Meng Y, Chen G and Huang M 2022 *Nanomaterials* **12** 1171
[11] Frit B, Mercurio J 1992 *J. Alloys Compd.* **188** 27
[12] Zhao Y, Li Y, Lu Y and Wang Y 2010 *Ferroelectrics* **404** 45
[13] Tan Z, Xi J, Xing J, Wu B, Zhang Q, Chen Q and Zhu J 2022 *J. Eur. Ceram. Soc.* **42** 3865
[14] Luo X, Yan Z, Luo H, Zhou X, Li B, Zhang M and Zhang D 2023 *Adv. Powder. Mater.* **2** 100116
[15] Xi J, Chen H, Peng X, Wan H, Lin Y, Tan Z, Xing J, Chen Q, Zhu J and Ye Z G 2023 *J. Am. Ceram. Soc.* **43** 4757
[16] Cui X, Zhao L, Wang J, Miao J and Zhao G J 2025 *Ceram. Int.* **51** 14132
[17] Chen Z, Zhang Y, Huang P, Li X, Du J, Bai W, Li L, Wen F, Zheng P and Wu W J 2020 *Ceram. Int.* **136** 109195
[18] Chen X, Ma Z, Li B and Dai Y 2024 *J. Adv. Ceram* **13** 263
[19] Zuo Y, Fang Z, Fan D, Liu K, Niu H, Wang H, Du Y, Shen M, Shang X and Li Z J 2022 *Ceram. Int.* **48** 9297
[20] Mo W, Luo X, Zhang Y, Niu H, Fang Z, Hu L, Liu K, Li Q, Chen Y and Shen M 2023 *J. Am. Ceram. Soc.* **106** 2466
[21] Xi J, Xing J, Yuan J, Nie R, Chen H, Zhang W, Chen Q and Zhu J 2020 *J. Mater. Sci.: Mater. Electron.* **31** 8805
[22] Long C, Fan H, Li M, Ren P and Cai Y 2013 *CrystEngComm* **15** 10212
[23] Long C, Xu A, Su Z, Ren W, Liu L and Ding X 2025 *J. Materiomics* **11** 100990
[24] Wang Q, Fan H, Long C and Huang L J 2014 *J. Mater. Sci.: Mater. Electron.* **25** 2961
[25] Dai H, Zhao K, Wang T, Wang J, Jiang H, Du P, Sun R and Luo L 2025 *Adv. Funct. Mater.* **36** e18029
[26] Qiu C, Wang Y, Jin R, Hu L, Xu Z, Geng L D and Yan Y 2025 *J. Am. Ceram. Soc.* **108** e20587
[27] Chen J N, Pei X Z, Wang Q, Zhao X, Wang Z Y and Wang C M 2025 *J. Eur. Ceram. Soc.* **45** 117065
[28] Shi W, Mo M, Hu Q, Tan Z, Guan S, Xu L, Xing J and Chen Q 2025 *Mater. Horiz* **12** 10314
[29] Sacks M D, Scheiffele G W and Staab G A 1996 *J. Am. Ceram. Soc.* **79** 1611
[30] Hong S H and Messing G L 1999 *J. Am. Ceram. Soc.* **82** 867
[31] Hong S H, Trolier-McKinstry S and Messing G L 2000 *J. Am. Ceram. Soc.* **83** 113
[32] Luo X, Wang M, Yuan X, Zhang Y, Zhou X, Luo H and Zhang D 2025 *J. Mater. Chem. A* **13** 2121
[33] Zhang G, Zhu D, Zhang X, Zhang L, Yi J, Xie B, Zeng Y, Li Q, Wang Q and Jiang S 2015 *J. Am. Ceram. Soc.* **98** 1175
[34] Guan S, Shi W, Wu X, Xu H, Wu Y, Lang R and Chen Q 2024 *J. Eur. Ceram. Soc.* **44** 2087
[35] Tokita M 2021 *Ceramics* **4** 160
[36] Li G-H, Wang Q, Zhang F, Yang Y K, Liu H T and Wang C M 2025 *J. Mater. Chem. C* **13** 9115
[37] Jiang D, Zhou Z, Liang R and Dong X 2021 *J. Eur. Ceram. Soc.* **41** 1244
[38] Luo J 2025 arXiv preprint 2510.05629
[39] Zhang Y, Chen L, Liu H, Deng S, Qi H and Chen J 2023 *InfoMat* **5** e12488
[40] Ding Q, Zhang Y, Chen X, Fu X, Chen D, Chen S, Gu L, Wei F, Bei H and Gao Y 2019 *Nature* **574** 223
[41] Zeng Y, Ouyang B, Liu J, Byeon Y-W, Cai Z, Miara L J, Wang Y and Ceder G 2022 *Science* **378** 1320
[42] Jiang B, Yu Y, Cui J, Liu X, Xie L, Liao J, Zhang Q, Huang Y, Ning S and Jia B 2021 *Science* **371** 830
[43] Wu J, Ma X, Zhou D, Qi H, Zhang R, Huo C, Chen L, Li H, Deng S and Fan L 2025 *Adv. Mater.* **37** 2419134
[44] Chen H, Jiang C, Wong V K, Lim D B K, Yin J, Tan Z, Yao K and Zhu J 2025 *Adv. Mater.* **305** 121870
[45] Wang W, Zhang Y, Ding D, Liang R and Zhou Z 2025 *Ceram. Int.* **51** 33673
[46] Fang W, Wu J, Qi H, Ma H, Zhou D, Yu H, Zheng Z, Guo J and Chen J 2025 *Acta Mater.* **293** 121108
[47] Wu Y, Chen N, Wang B, Cheng Y, Shi W, Cong Z, Tan Z, Xing J and Zhu J 2026 *Phys. Status Solidi RRL* **20** e202500411